Collision induced spatial organization of microtubules

Vladimir A. Baulin *, Carlos M. Marques, Fabrice Thalmann

Institut Charles Sadron CNRS UPR 22, 67083 Strasbourg Cedex, France

Abstract

The dynamic behavior of microtubules in solution can be strongly modified by interactions with walls or other structures. We examine here a microtubule growth model where the increase in size of the plus-end is perturbed by collisions with other microtubules. We show that such a simple mechanism of constrained growth can induce ordered structures and patterns from an initially isotropic and homogeneous suspension. We find that microtubules self-organize locally in randomly oriented domains that grow and compete with each other. A weak orientation bias, similar to the one induced by gravity or cellular boundaries is enough to influence the domain growth direction, eventually leading to a macroscopic sample orientation.
© 2007 Elsevier B.V. All rights reserved.

1. Introduction

Biological processes like cell division, transport of certain organelles, morphogenesis and organization in the cell are mediated by rod like structures known as microtubules, which form various arrays, radial spindles, parallel and anti-parallel bundles [1–3]. The microtubule self-assembly in living organisms is regulated by different factors: microtubule-associated proteins (MAPs) which stabilize, destabilize and crosslink microtubules [4,5], diverse kinesin-like motor proteins, which organize and link microtubules, γ-tubulin ring complex which serves as a template for nucleation sites for microtubule polymerization in centrosomes [6,7]. These factors combine with the physical and chemical properties like ionic concentrations, temperature and pH to determine, by mechanisms not yet well understood, the spatial structure and the orientation of the microtubules.

Each individual microtubule is a highly dynamic self-assembled rod, which is permanently growing or shrinking. This ability for being in an everlasting state of length change has won microtubules the name of "searching devices" for specific targets in the cell [3,8]. A key property allowing for this bistable state is the dynamic instability [4]. Due to conformational asymmetry of the constituting microtubule subunit, the hetero-

dimer α,β-tubulin, a microtubule has a polar structure which leads to differences in addition rates: in average there is a net addition of monomers at plus-end and net removal at minus-end. The speed of growth at the plus-end is not constant, but rather intermittent. The elongation of the plus-end is stochastically alternated by the abrupt shrinking, in a process of unidimensional diffusion [9]. Such dynamic behavior is attributed to the complex, two-stage assembly of the plus-end, implying the internal hydrolysis of the GTP in a tubulin dimer. Within the cap model [4,5,10], the tubulins added to the growing plus-end are not hydrolyzed, thus having configurations favorable for the microtubule assembly. They presumably form a cap preventing the plus-end from the disassembly and shrinking. Once incorporated into microtubules GTP-tubulins eventually hydrolyze. During conversion of the GTP of β-subunit to the GDP, the tubulin heterodimer undergoes the conformational change that destabilizes the tubular structure of a microtubule and favors shrinking [11]. Above some threshold concentration of GTP the microtubules grow at a constant speed, while below this concentration the microtubules lose their stabilizing cap and shrink, a phenomenon known as catastrophe. In solution the GDP from the disassembled tubulin can be regenerated to GTP capable to participate again into the formation of new microtubules. The competition between the rates of internal and external hydrolysis may lead to a complex collective behavior. The growth of microtubules at high concentrations of GTP may abruptly change to shrinking when the GTP is exhausted and later resume if new GTP becomes available. Such

* Corresponding author. Present address: Universitat Rovira i Virgili 26 Av. dels Països Catalans Tarragona 43007, Spain.
E-mail address: vladimir.baulin@urv.cat (V.A. Baulin).

collective behavior can lead to microtubule mass oscillations and pattern formation [12–14].

Different examples of spontaneous self-organization of dynamic microtubules have been reported in the literature [15–20]. They describe the in-vitro formation of spatial structures in a solution of microtubules that start growing from seeds distributed homogeneously and end-up organized as highly aligned strips. The resulting pattern is sensitive to the direction of the gravitational field. Interestingly, the observed structures do not appear in weightlessness conditions [15]. The authors conclude from their observations that the Earth gravity only triggers the symmetry breaking and does not affect individual microtubules. The coupling of gravity with the usual excluded volume effects known in liquid crystals is not sufficient to cause the system orientation [21,22]: the shaking or mixing of the sample irrevocably destroys the pattern. Since the in-vitro preparation does not contain any molecular motors or MAPs, the self-organization in stripes is attributed to the dynamic nature of microtubules: the pattern formation disappears when the dynamic instability is inhibited by the addition of taxol. Similar patterns are formed under magnetic fields [17].

In the present study we propose an alternative mechanism for the microtubules spatial organization and pattern formation. It is based on two experimental facts: (i) interaction of microtubules with boundaries alters the growth rate. Experiments involving growing microtubules and different immobile obstacles and barriers have shown that the opposing force increases the catastrophe rate and reduces the growth velocity [23,24]. The boundaries may also induce the orientation preference. This is likely due to a higher catastrophe rate in the direction perpendicular to the boundary than along the boundary. Recent in-vivo work suggests that the microtubule dynamic instability is altered during preprophase band formation [25]. Microtubule reorientation is accompanied by the increase of the catastrophe frequency and growth rate, while the rescue frequency and shrinkage rate remain unchanged. The experimental study of the microtubule self-organization in miniature containers of different geometries and in phospholipid vesicles [20] clearly shows the dependence of the pattern on the boundaries. The gradients always present in living cells can also play the role of an "effective" boundary and induce the microtubules ordering [26]. (ii) Inter-microtubules collisions affect their dynamic behavior [27]. In vivo observation of collisions between individual cortical microtubules shows that the steep contact angles of microtubules collisions provoke catastrophes more often than the shallow contact angles, while the microtubules with close angles have shown a tendency to zippering into bundles. The collisions between individual microtubules can also lead to local ordering: in-vivo observations of the reorientation of cortical microtubules in parallel arrays suggest that the collision induced depolymerization of disordered microtubules is followed by their repolymerization into ordered arrays [28–31].

Inspired by the available experiments and results, we propose the simplest possible physical model that couples growth and orientation through intermicrotubule collisions. In the next section we set the foundations for the physical model. In Section 3 we show numerically that this mechanism alone leads to the orientation of microtubules in aligned stripes. A theoretical discussion of our main results is presented in Section 4 and our findings are summarized in the conclusion.

2. The model

2.1. A kinetically constrained growth model

We propose a model based on the assumption that the assembly dynamics of a particular microtubule is influenced by others microtubules in the close neighborhood. A microtubule is modeled as a rigid, oriented rod which shrinks at its minus-end and grows at its plus-end. The dynamic properties of microtubules are coarse-grained: instead of dealing with a fluctuating rate of growth and shrinking associated with catastrophe and rescue events, we rather consider smooth, averaged properties, namely the *average* speeds of growth and shrinking. Without obstruction, in a free environment, the plus-end of a microtubule grows at constant speed v^+, while its minus-end shrinks at constant speed v^-. When the plus-end encounters another rod, it stops, but the rod continues to shrink at its minus-end, with speed v^-, and as a result, the overall length of the rod decreases. The rod resumes its growth as soon as the plus-end is no longer blocked by its neighbor. Altogether, the plus-end experiences an environment dependent intermittent growth, and the minus-end a constant motion at speed v^-. The rod disappears if its length decreases to zero during the shrinkage phase. The rod orientation is never changed during its life. The total number of rods is not fixed, but is maintained by a permanent and constant injection rate of new rods at random positions, with random orientation and zero length. Such a simplified model allows us to reduce the number of parameters to two: the injection rate and the ratio of the speeds of growth and shrinkage.

We found that this mechanism of constrained growth alone can lead to spontaneous alignment of microtubules from an initially isotropic and homogeneous array. The emergence of a local orientational order is reminiscent from a natural selection process. Whenever some local anisotropy builds up, the survival rate of the neighboring rods changes and becomes orientation dependent. The rods which from the start have picked up the dominant orientation are likely to outlive rods with a different orientation, and this creates conditions favoring the population of rods with the "correct" orientation at the expense of rods with "incorrect" orientation. In our model, the rods cannot change their orientation but the permanent injection of young, randomly oriented rods, leaves to the system the possibility to reorganize and to tune up to a change of external conditions.

We implemented numerically this constrained growth model. The simulations clearly show a trend towards some local organization and ordering, with the formation of well defined anisotropic domains.

2.2. Numerical implementation of the constrained growth model

In our numerical implementation, in two dimensions, each rod is characterized by its length, its position, and its orientation. The orientation (one angle) and the position (two coordinates) are set

when the rod is injected, and do not change until the rod eventually disappears. The length of each rod evolves with time, starting from zero shortly after the injection. All rods are packed in a square box of side L_s, subject to periodic boundary conditions.

Depending on their dynamic state, the rods belong to two categories: shrinking rods (s-rods) are the rods that the local environment prevents from growing further (kinetic constraint), while growing rods (g-rods) are free to grow.

The rule for the time evolution of the rods is the *non-crossing displacement*. Updates are done every time interval Δt. The minus tip of each rod is shortened by the amount $v^- \Delta t$, while the plus tip attempts a move forward by $v^+ \Delta t$. If this move can be done without crossing any other rod, the move is accepted and the rod grows. If the rod was in a s-rod state, it converts to a g-rod state. Otherwise, the move is rejected, and the rod switches to, or stays in a blocked s-rod state. As a result, the length of a rod after each step, either increases by $(v^+ - v^-)\Delta t$, or decreases by $v^- \Delta t$.

In order to stick as close as possible to the in-vitro experimental results, we set our unit length to 0.1 μm and our unit of time to 0.1 s. However this model is to a large extent scale invariant which means that its length and time-scales can be fixed arbitrarily without changing the model main behavior. In the present case, we chose the values $L_s = 10$ μm and $\Delta t = 0.1$ s. The speed v^+ ranges from 0.5 μm s^{-1} to 2.1 μm s^{-1} and $v^- = 0.3$ μm s^{-1}. In the discussion, we make a frequent use of the dimensionless speed ratio α:

$$\alpha = \frac{v^-}{v^+ - v^-}, \tag{1}$$

defined as the ratio between the speed of shrinkage in the s-state v^- and the speed of growth in the g-state $v^+ - v^-$. The corresponding values of α used in the simulation lie in the interval 0.17 to 1.5. The value for the injection rate Q_i is about 100 new rods per μm^2 and per second, corresponding to the injection of 1000 new rods in the box at each time step of the simulation. There are typically a few thousand rods (1000 to 50 000) at any time in the simulation box. These values roughly correspond to experimental data (see e.g. [32]). With this set of parameters the ordering arises after ∼ 10 000 steps corresponding to several minutes.

3. Main results

3.1. Spatial organization: domain structure

The simulation starts with a set of rods of zero length. The kinetic constraint concerns a vanishingly small number of rods at the early stage of the system evolution. As the number and the length of the rods increase, the amount of packing gets larger, and the kinetic constraint forces a significant fraction of rods into a blocked, shrinking state. This transient regime recedes to a quasi-stationary regime in which the ratio of s-rods and g-rods seems to remain approximately constant.

Then, the numerical simulations show clearly the slow emergence of oriented domains, or bundles, of nearly aligned rods. These domains show very rough, ragged and sharp boundaries,

much as crystallites. Thus, they look quite different from the domains arising in the usual phase transitions and coarsening situations, where a finite bending elasticity creates a smooth variation of the order parameter, at the vicinity of a domain wall. The domains seem to be randomly oriented, and the isotropy of the system is recovered only on length scales larger than the size of the domains.

In the final stages of the simulation, the average domain size $L(t)$ is still a slowly growing function of the time, and eventually becomes of the same order of magnitude as the size of the system L_s. This prevents reaching an asymptotic finite value of $L(t)$, associated to a truly stationary distribution of the rod lengths and orientations. Well known examples of such coarsening dynamics are characterized, for instance, by a power-law or a logarithmic behavior of L with t [33]. In the latter case, the possibility to discuss the system properties in term of quasi-stationary solutions remains.

Fig. 1 illustrates how the rods self-organize with time. At first, the population of rods is isotropic, except for small fluctuations inherent to the random initial position and orientation distribution (Fig. 1a). These pre-existing heterogeneities grow into small bundles, whose distribution still remain seemingly isotropic on large scales (Fig. 1b). Then, larger bundles emerge at the expense of many other smaller bundles, bound to disappear (Fig. 1c). Finally, the typical size of the larger bundles becomes comparable to the size of the simulation box (Fig. 1d). The absence of bending modulus, and the presence of ragged boundaries, forbids a mechanism based upon domain walls motion. Such a competitive growth of the domains is slow. In our model we have only two parameters: the relation of speeds of growth and shrinkage and the injection rate. The formation of ordered domains is very robust to change in these parameters. The patterns and characteristics of the ordered structures differ only quantitatively.

To quantify the degree of local ordering, or "polarization", of the system, we introduce a dominant angle Θ, which maximizes a cost function σ:

$$\sigma(\theta) = \frac{1}{n_t} \sum_{i=1}^{n_t} \cos^2(\Omega_i - \theta), \tag{2}$$
$$= \overline{\cos^2(\Omega - \theta)}$$

where Ω_i is the orientation (angle) of the ith rod, and the sum runs over n_t, the total number of rods present in the system. Thus, σ is defined as the "ensemble average" over the population of rods at time t, denoted with an overline $\overline{...}$. We call order parameter the value of the maximum $s = \sigma(\Theta)$. The cost function can be expanded as $\sigma(\theta) = \overline{\cos^2\Omega}\cos^2\theta + \overline{\sin^2\Omega}\sin^2\theta + \overline{2\sin\Omega\cos\Omega}\sin^2\theta$. Then, the stationarity condition $\partial\sigma(\theta)/\partial\theta|_\Theta = 0$ leads to:

$$\tan 2\Theta = \frac{\overline{\sin 2\Omega}}{\overline{\cos 2\Omega}}. \tag{3}$$

This equation has always four solutions, two corresponding to the maxima Θ_{max} and $\Theta_{max} + \pi$, and the other two, to the minima Θ_{min} or $\Theta_{min} + \pi$, and Θ_{max} and Θ_{min} are mutually orthogonal.

A scaled anisotropy parameter S may be defined as:

$$S = \frac{\sigma(\Theta_{max}) - \sigma(\Theta_{min})}{\sigma(\Theta_{max}) + \sigma(\Theta_{min})}. \tag{4}$$

The quantity S is 0 for a population of isotropically oriented rods, while it is 1 for a population of perfectly aligned rods. The parameter S makes it possible to quantitatively assess the amount of ordering in the system. Because both parameters s and S turn out to fluctuate strongly with time, we introduce a more stable parameter, where each rod i contributes according to its length l_i:

$$\sigma_l(\theta) = \frac{1}{n_t}\sum_{i=1}^{n_t} l_i^2 \cos^2(\Omega_i - \theta), \tag{5}$$

where the long rods participate more than the short ones. The dominant angle associated with this parameter obeys:

$$\tan 2\Theta_l = \frac{\overline{l^2 \sin 2\Omega}}{\overline{l^2 \cos 2\Omega}}, \tag{6}$$

and the anisotropy ratio S_l defined as in Eq. (4), with σ replaced by σ_l.

Fig. 2 shows the variation of the dominant angles Θ and Θ_l with time, for one set of parameters. At the beginning, the system is homogeneous and the distribution of angles is isotropic, resulting in a singular and noisy function of time. As
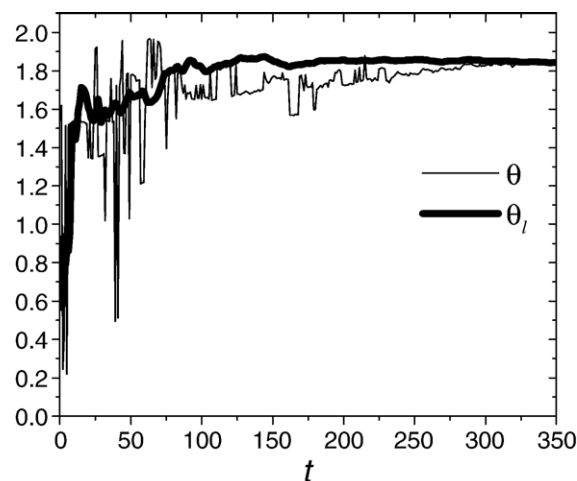
Fig. 2. The dominant angles Θ, Θ_l as a function of the time, as found by minimizing Eqs. (3) and (6).

the system evolves, the ordered structures appear and the angles stabilize around their preferred value. It is noteworthy that the Θ_l curve is smoother than the Θ curve, due the stabilizing contribution of the longest and most stable rods. The plateau value is related to the orientation of the dominant bundle, and fluctuates from sample to sample.

The same conclusion can be drawn from the plot of the anisotropy ratios S and S_l, function of time in Fig. 3. Although
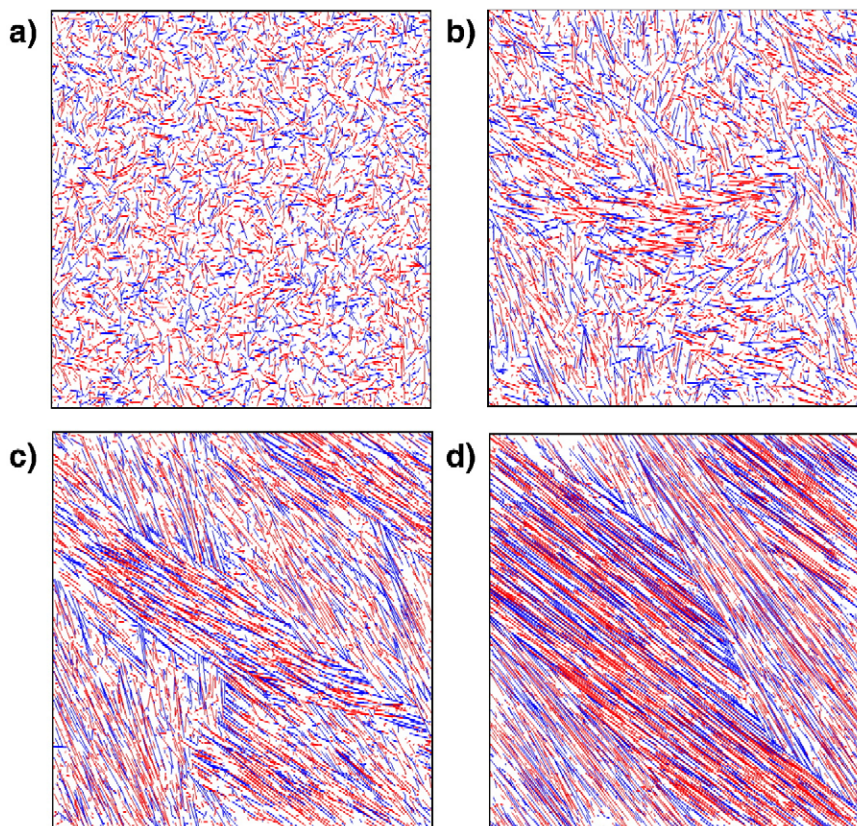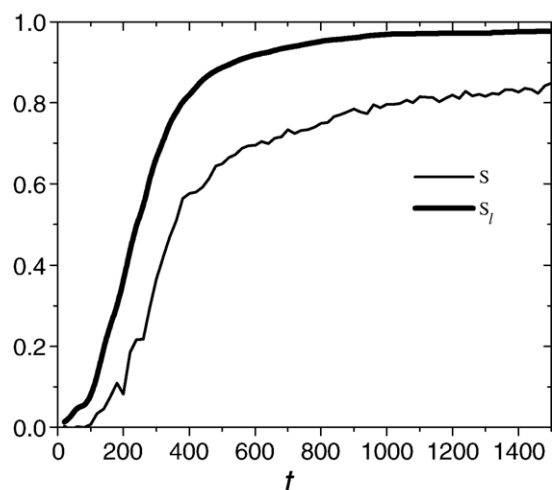
Fig. 1. Snapshots of the system in 2D of rods at various successive times (time increases from a to d). Growing rods are drawn in blue, and shrinking rods in red. (For interpretation of the references to color in this figure legend, the reader is referred to the web version of this article.)

Fig. 3. Anisotropy ratios S_l and S vs. time t.

Fig. 4. The anisotropy ratio S_l vs. time, for three increasing biases in the angular distribution of the rods orientation.

evolving on the same time scale as S, the quantity S_l reaches a value closer to 1. The difference between the two curves is most certainly due to the contribution of the many young, short rods, upon which the kinetic constraint has not been acting long enough to force them into the dominant orientation.
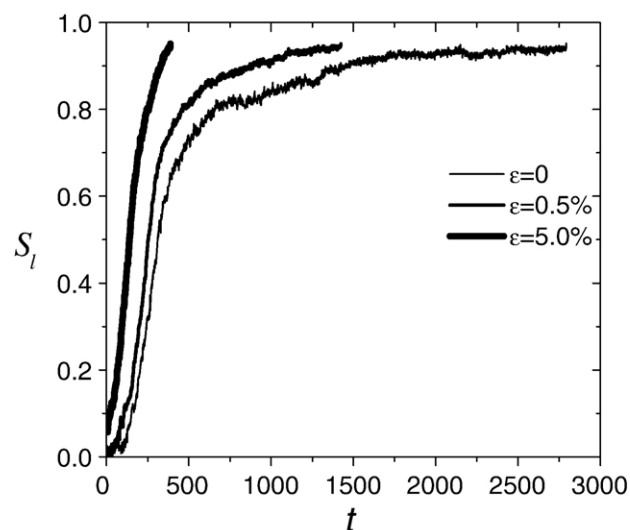
The anisotropy ratio and the dominant angles aim at quantifying the degree of local ordering in a suspension of rod like objects, irrespective of the underlying alignment mechanism. In that respect, they make possible a direct comparison with other alternative models of microtubule orientation. From these curves, one can infer a characteristic time t^* for the emergence of a global orientation in the sample, such as, for instance, $S_l(t^*)=1/2$. In Fig. 3, this ordering time is about a few hundred steps ($t^* \sim 300$).

3.2. Sensitivity to external stresses

The constant renewal of the rods, along with the growth of the competing domains, confers to the system the ability to respond to external perturbations. One of our main motivations is to evaluate the sensitivity of the ordering to the presence of an external gravitational, or magnetic field. Quite similarly, the presence of a hard wall is expected to align the nearby domains along its direction.

In order to probe the ability of the rods suspension to cope with external constraints, and to monitor its susceptibility to a small symmetry breaking, we performed several simulations with a slightly biased distribution in the orientation of the newly injected rods. Instead of being isotropic, we added a fraction of rods in excess, with an angle Ω belonging to a small interval $\Omega_0 \pm 1°$. As a result, a value $\epsilon=0.5\%$ brings about an acceleration of the ordering time t^* by a factor 1.5, and a value $\epsilon=5\%$ triggers a three times faster growth of the domains (Fig. 4). In both cases, the preferred orientation is clearly related to the orientation of the bias Ω_0.

Boundaries and impurities can also induce the alignment. When one of the periodic boundary conditions is replaced by a hard wall, the alignment of the rods is much faster, and the wall orientation propagates into the bulk of the suspension. An

identical behavior is observed when a rod with fixed length, position and orientation, is forced into the simulation box. The rods orient themselves parallel to the guiding rod, and longer guiding rods provoke faster ordering.

3.3. Kinetics of individual rods

The numerical simulation makes it possible to track a single rod as it evolves with time. We observe that during its life cycle, a rod can experience many alternating periods of growth and shrinkage. A typical microtubule life history plot is shown in Fig. 5, following a saw-teeth curve.

We call "age" T, the time interval elapsed since the rod was injected with zero length in the system. The age is the sum of the
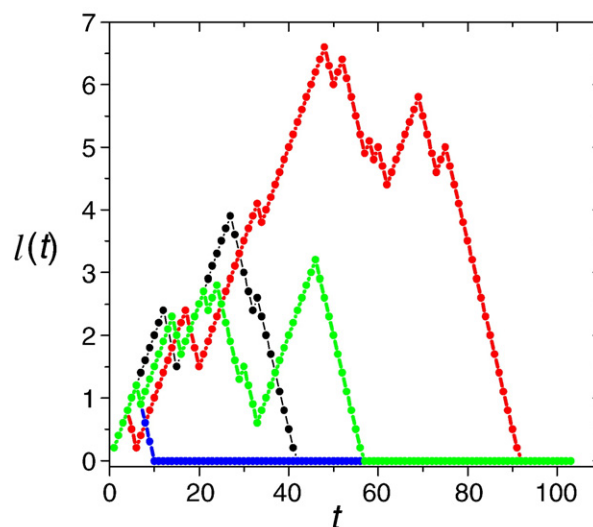
Fig. 5. Different rod histories, showing the length $l(t)$ function of the time t. The curves are similar to random walks with an absorbing boundary condition at $l=0$.

growing time T^+ and the shrinking time T^-, and the length of the rods can be expressed with the help of T^+, T^- as

$$
\begin{aligned}
l &= (v^+ - v^-)T^+ - v^-T^-; \\
T &= T^+ + T^-,
\end{aligned}
\tag{7}
$$

or equivalently,

$$
T^- = \frac{(v^+ - v^-)T - l}{v^+}; \; T^+ = \frac{v^-T + l}{v^+}.
\tag{8}
$$

A typical distribution of both T^+ and T^-, as a function of the age T, is shown in Fig. 6 for a population of rods at a given time t (scatter plot), while the inset of Fig. 6 is an enlargement of this plot in the small T region. The values T^+ and T^- of old rods (large T), concentrate near two boundaries, which correspond to a length $l=0$ in Eq. (8). For these old rods, which have survived many collisions, the growth and shrinkage periods compensate almost exactly, and in Eq. (7), the length l results from the difference between two large quantities. By contrast, the young rods (small T) show all possible combinations of T^+ and T^- (inset in Fig. 6). This indicates that the young rods have not yet been influenced by their surrounding. The maximal possible length of a rod occurs in the extreme case $T^-=0$ and $T^+=T$, thus corresponding to a length $l_{max}=(v^+ - v^-)T$ (the dashed line in the inset of Fig. 6).

Young rods enjoy a fast growth rate, but many are also eliminated quickly. Older rods show a smaller average growth rate, but their survival rate increases with their age. This is clear from the histogram of the ages, which is clearly not exponential, but rather well approximated by a power law $p_s(T) \sim T^{-1}$ (Fig. 7). The relative disappearance rate of rods aged T, is $p^{-1}dp_s/dt \sim T^{-1}$, instead of remaining constant, as in the exponential case (e.g. like for instance the decay of radioactive elements).

In a sense, the young rods shows "plastic" properties, and account for the adaptability properties of the rods suspension. By contrast, older rods are expected to show more rigidity and persistence from the past history of the suspension. We did not find any simple justification for the exponent -1, which is a
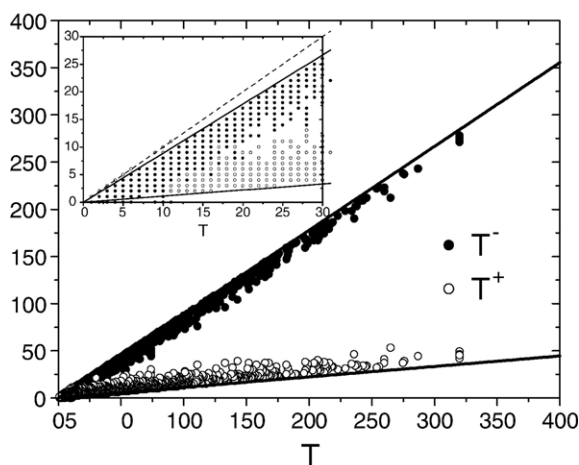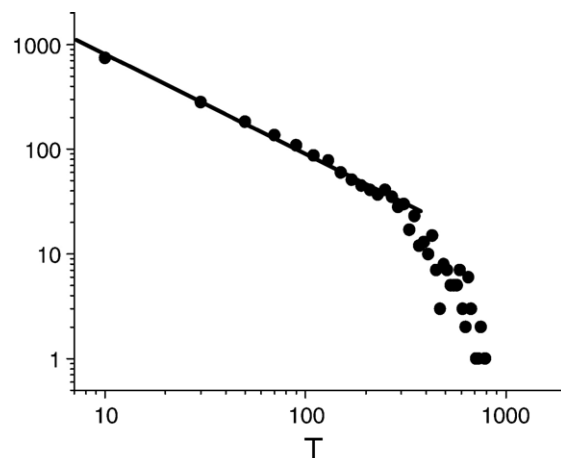

Fig. 7. Histogram of the distribution of the ages T of a population of rods, in logarithmic coordinates. The initial decay rate is close to $1/T$, followed by an exponential decay.

numerical finding. This contradicts a naive argument based on the usual random walks, which would predict a $T^{-3/2}$ behavior associated to the first return to the origin time distribution. We still believe in the analogy, but we attribute this discrepancy to the existence of strong correlations between orientation, age and life time of the rods. Finally, the age of the very old rods is distributed exponentially (Fig. 7).

A scatter plot of the lengths l vs. the ages T of a population of rods does not support the presence of strong correlations between these two parameters (Fig. 8).

3.4. Distribution of lengths and orientations

The ordered structures (bundles or domains) effectively select the rods, keeping only those with an orientation compatible with the dominant orientation of the bundles. The correctly oriented rods collide less often with their neighbors than the rods with transverse orientations, and their "fitness", or survival ability is greater.

Fig. 9 shows three typical scatter plots of the ages as a function of the angles. The age of the system increases from the

Fig. 6. Scatter plot of the times of growth T^+ and T^-, as a function of the total age $T=T+T^-$, for a given population at time t. Inset: a close-up look at the region of young rods.
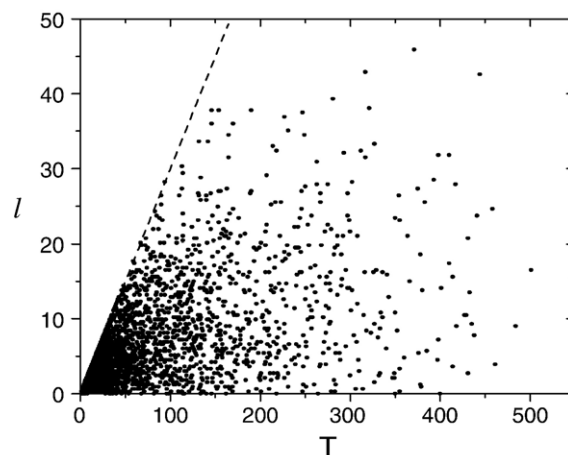

Fig. 8. Scatter plot of the length (vertical axis) and the age (horizontal axis).
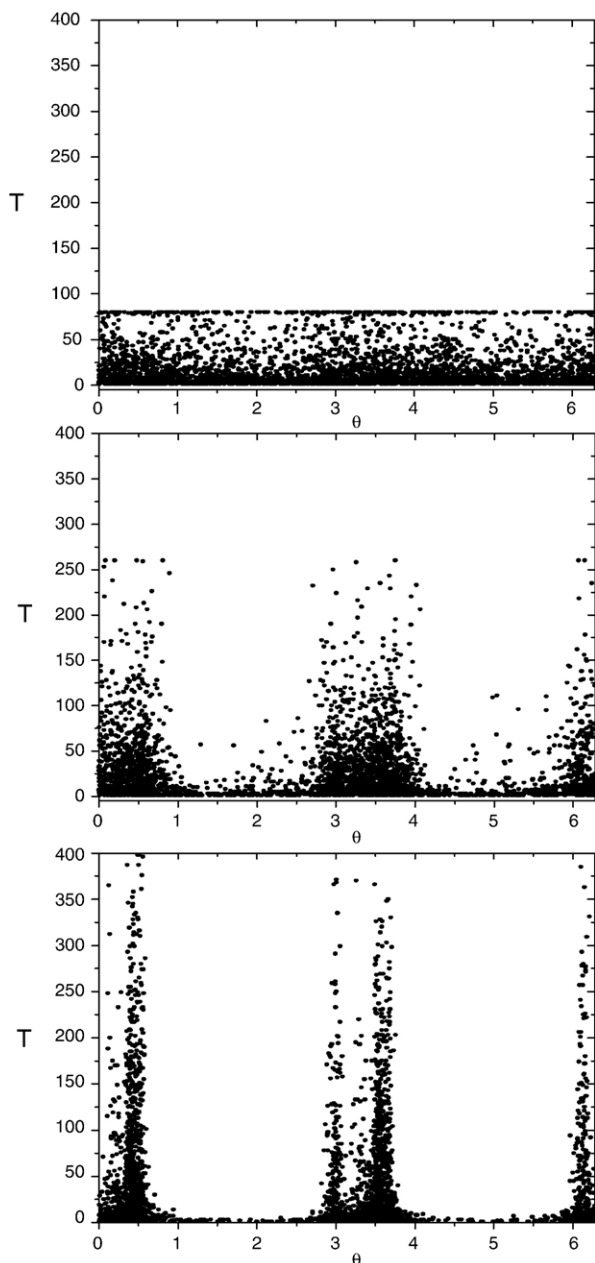
Fig. 9. Scatter plot of the orientation (horizontal axis) and the age (vertical axis) of the rods at three different stages of the evolution of the system. The time t increases from top to bottom.

top to the bottom plot. The presence of anisotropic domains manifests itself as sharp peaks around a few well defined angles. On the example shown, one can see two different domains, respectively around 25° and 160°. The peaks are duplicated (mirrored) because the bundles contain a mixture of two anti-parallel populations, separated by 180°.

A typical distribution of lengths regardless to the rods orientation is shown in Fig. 10. The distribution is exponential except for a very small region of tiny lengths. Most of the rods with tiny lengths are very young rods injected in the system a few steps ago. They did not have time to experience collisions and their distribution did not acquire the same characteristics as the old rods.
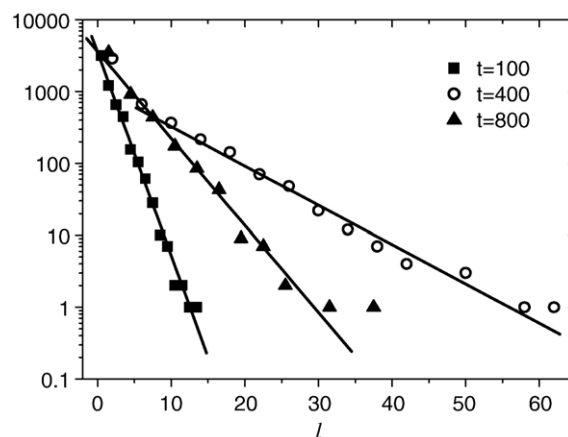

Fig. 10. Semilogarithmic plot of the histogram of rods lengths, for three different stages of the evolution of the system. Straight lines correspond to an exponential decay.

The system not only adjusts the orientation and the length of the rods, but it also regulates the total number of rods n_t. The injection rate stays constant during the simulation. In the early stage of the simulation, in a sparse system, the newly injected rods do not meet any obstacles and the total number of rods increases sharply. An increase in the rods density leads to a higher collision rate among rods, and a higher elimination rate. After a transient regime, n_t evolves very slowly, although it is not strictly constant. As a matter of fact, n_t slightly decreases with the spreading of the dominant orientation and the emergence of domains (Fig. 11) while the total mass increases until reaching the plateau corresponding to this quasi-stationary state. In this regime the injection rate becomes equal to the loss of tubulin due to shrinking.

3.5. The three dimensional case

Finally, we performed a limited number of simulations in three dimensions, in order to check whether the kinetic ordering
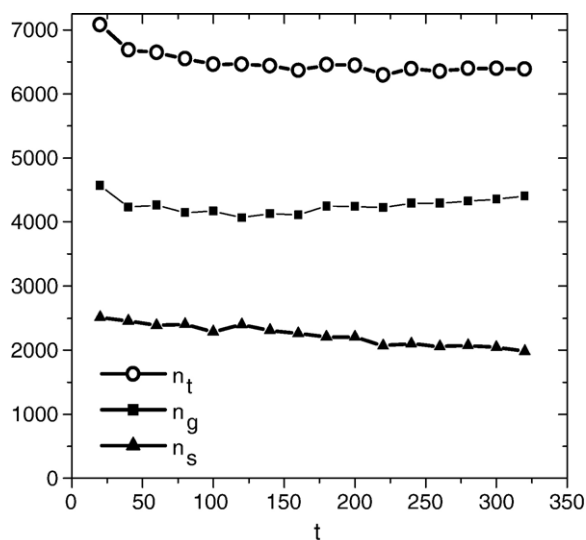

Fig. 11. Evolution of the number of rods n_t with time, and repartition between shrinking rods (n_s) and growing rods (n_g).
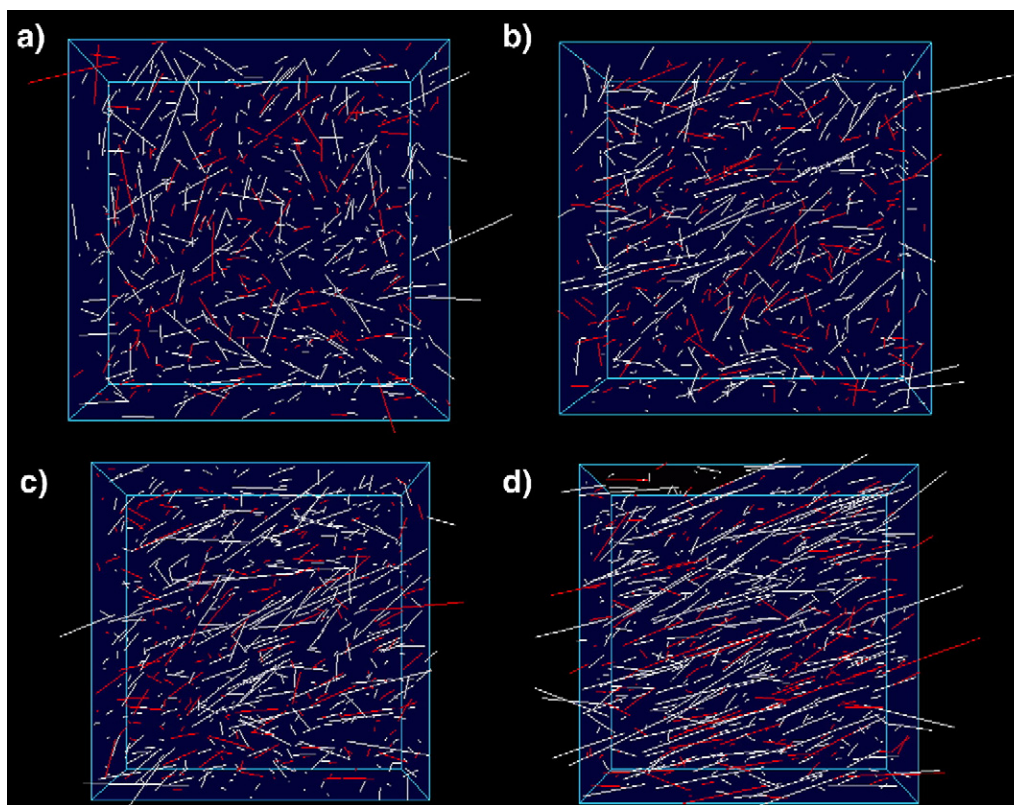
Fig. 12. Snapshots of the system of rods in 3D at various successive times (time increases from a to d). Growing rods are drawn in white, and shrinking rods in red. (For interpretation of the references to color in this figure legend, the reader is referred to the web version of this article.)

was a special feature of the two dimensional systems, or whether it was a generic feature also in three dimensions. In this case, our simulation box is a cube of size $100 \times 100 \times 100$. In addition to the injection rate Q_i, to the speeds v^+ and v^-, there is another relevant parameter: the diameter, or thickness, of the rods d. A typical snapshot is presented in Fig. 12.

It turns out that the behavior of the system in three dimensions is quite similar to the one observed in two dimensions. The initially homogenous solution becomes gradually structured into bundles and domains. However, the three dimensional system differs by the absence of sharp boundaries between domains. The competition between the different orientations is not so drastic, since bundles with different orientation can interpenetrate if the rod thickness is small. Domain walls are more difficult to identify, but the main result, i.e. local ordering, holds also in three dimensions.

4. Theoretical discussion

We discuss in this part some observed features of our numerical simulations: exponential tails in the length distribution, collision rates, anisotropy. For this purpose, we propose an elementary kinetic theory, and its predictions are compared with the numerical simulations.

4.1. Ensemble and time averages

Much like in the usual statistical mechanics, one introduces two kinds of averages. The time average, denoted by brackets

$\langle \ldots \rangle$ corresponds to the mean value obtained by the repeated observation of single rods evolving with time. For instance, $\langle T^+ \rangle$ is the average growth time of a rod. Time averages are accessible through numerical simulations.

The ensemble average amounts to considering the whole population of rods at a given time. This corresponds to an instantaneous "snapshot" of the population of rods, and the corresponding average is denoted with an overline $\langle \overline{\ldots} \rangle$: for instance, $\bar{l}$ is the average length of the rods. In practice, the ensemble average consists in summing over all the rods, and then dividing by their total number n_t. The ensemble averages can be computed from the simulations, but are also the natural outputs of the kinetic theory sketched below.

The connection between time and ensemble average is by no means obvious. In the case of a true stationary situation, both averages are expected to coincide. Our situation, however is not a full stationary situation, as we witness the emergence of unbounded large bundles. A slow coarsening dynamics, however, may still exhibit a satisfactory agreement between the two kinds of averages.

Ensemble averages are conveniently handled by means of distribution functions. Denoting the length, orientation and position of the rods respectively by l, Ω and $\vec{r}$, we define $c_t(l, \Omega, \vec{r}, t) = c_g(l, \Omega, \vec{r}, t) + c_s(l, \Omega, \vec{r}, t)$, where c_g, c_s and c_t stand respectively for the distribution of the population of growing rods, shrinking rods and total number of rods, per unit of surface, at time t, with $0 \leq l < \infty$, $0 \leq \Omega < 2\pi$ and position $\vec{r}$.
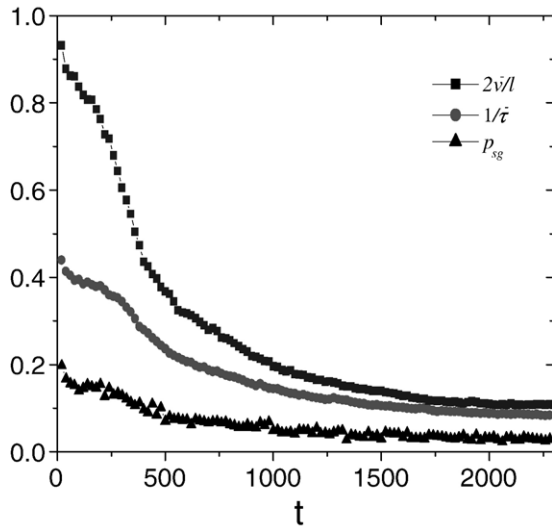
Fig. 13. Test of the relations Eqs. (14) and (B.7). Circles: inverse of the average shrinkage interval $\langle \tau \rangle$, last term of Eq. (18), squares: r.h.s. of Eq. (14), triangles: computed value of p_{sg}.

Successive integrations over the variables $\overrightarrow{r}$, l or Ω, give rise to a hierarchy of distribution functions. In particular, the numbers of rods n_s and n_g are given by:

$$n_g(t) = \int d\overrightarrow{r}\, dl\, d\Omega\; c_g(l, \Omega, \overrightarrow{r}, t); \tag{9}$$

$$n_s(t) = \int d\overrightarrow{r}\, dl\, d\Omega\; c_s(l, \Omega, \overrightarrow{r}, t). \tag{10}$$

In what follows, we use a loose notation for the partial distribution functions, where the variables which do not explicitly appear in c_g have been implicitly integrated over, e.g. $c_g(l, \Omega) dl d\Omega$ stands for the fraction of g-rods, with length between l and $l+dl$, angle between Ω and $\Omega+d\Omega$, but located at any position $\overrightarrow{r}$ of the system.

4.2. The distribution of lengths

Following the lines of Appendix A, we restrict ourselves to the homogeneous, $\overrightarrow{r}$-independent case, and assume that the distributions c_g and c_s comply with the following master equation:

$$\begin{cases} \dfrac{\partial}{\partial t} c_g + v \dfrac{\partial}{\partial l} c_g = p_{sg} c_s - p_{gs} c_g; \\ \dfrac{\partial}{\partial t} c_s - \alpha v \dfrac{\partial}{\partial l} c_s = p_{gs} c_g - p_{sg} c_s. \end{cases} \tag{11}$$

The properties of the distributions mostly depend on the injection rate Q_i, the speed $v = v^+ - v^-$, and the speed ratio $\alpha = v^- / (v^+ - v^-)$. We introduce the interconversion rates $p_{sg}(\Omega)$ and $p_{gs}(\Omega)$ between s and g-states, and we take care of a possible dependence on the direction Ω. We find that, for an homogeneous and stationary system, the lengths are exponentially distributed and verify:

$$c_g = \frac{Q_i}{v} \exp[-l/\overline{l}(\Omega)]; \tag{12}$$

$$c_s = \frac{Q_i}{\alpha v} \exp[-l/\overline{l}(\Omega)]. \tag{13}$$

Such an exponential distribution can be seen in Fig. 10. This model accounts for the possibility of anisotropic length distributions, via the angle dependent function $\overline{l}(\Omega)$. It is possible to find an isotropic, self-consistent solution for $\overline{l}(\Omega)=\overline{l}$, but we found also evidence for an anisotropic self-consistent solution, with a non-trivial function $\overline{l}(\Omega)$.

Our predictions for the isotropic solution include a determination of the rate p_{sg}:

$$p_{sg} = \frac{2v^-}{\overline{\overline{l}}}, \tag{14}$$

a determination of the rate p_{gs}:

$$p_{gs}(\Omega) = v^+ \frac{2\overline{l}}{\pi} \left(\frac{n_t}{S} \right), \tag{15}$$

and a self-consistent determination of the average length $\overline{l}$, as a function of Q_i, α, the total number of rods n_t and the surface S:

$$\overline{l} = \sqrt{\frac{3\pi}{2(\alpha+1)} \frac{S}{n_t}} \simeq \left(\frac{S}{n_t} \right)^{\frac{1}{2}}. \tag{16}$$

The predictions of Eq. (14) are shown in Fig. 13 and discussed also in Appendix B. Agreement is poor for short times and it improves for long times.

The predictions of Eqs. (15) and (16) are summarized in Fig. 14. The agreement is good for p_{gs} and qualitative for $\overline{l}$ at short times. The prediction becomes poor for times larger than t^*, associated to the emergence of the domains. We believe that the disagreement is mainly due to the impossibility for a two-dimensional system to be at the same time considered as anisotropic and homogeneous. By contrast, this would be a more reasonable assumption in a three dimensional space. Our kinetic theory shows too strong mean-field features to be able to describe accurately this two-dimensional situation. We conclude that the predictions of this isotropic model are no longer valid when the domains start growing.
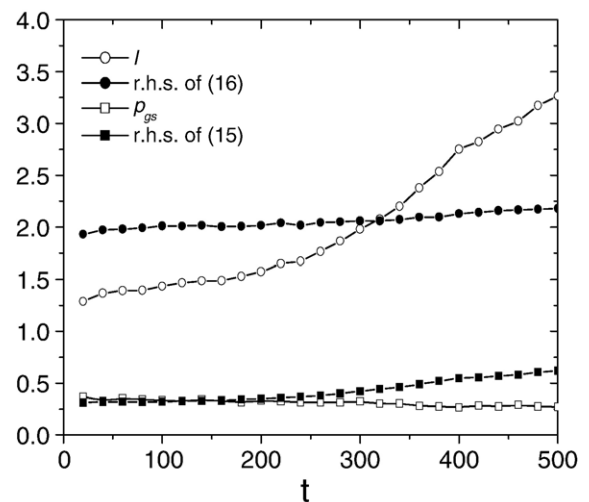

Fig. 14. Test of the relations Eq. (15) and (16). Open circles: l, filled circles: r.h.s. of Eq. (16), open squares: p_{gs}, filled squares: r.h.s. of Eq. (15).

4.3. Connections with the individual history of the rods

On the graph showing the individual life history of the rods (Fig. 5), one can decompose the time of growth T^+ into a sum of elementary growth intervals τ_j^+, and the time of shrinking T^- into a sum of elementary shrinking intervals τ_j^-:

$$T^+ = \sum_j \tau_j^+ ; T^- = \sum_j \tau_j^- . \tag{17}$$

In particular, we expect that the following relations between the average elementary time of growth $\langle \tau^+ \rangle$, shrinkage $\langle \tau^- \rangle$, and the rates p_{gs} and p_{sg} hold for an isotropic system:

$$p_{gs} = \langle \tau^+ \rangle^{-1} ; p_{sg} = \langle \tau^- \rangle^{-1} . \tag{18}$$

For an anisotropic system, p_{gs} becomes orientation dependent, while p_{sg} should not. In a stationary case, the following "detailed balance" relation holds:

$$n_g p_{gs} = n_s p_{sg}, \tag{19}$$

while in a quasi-stationary state, we expect only a qualitative relation:

$$\frac{n_g}{n_s} \simeq \frac{p_{sg}}{p_{gs}}, \tag{20}$$

suggesting the relation:

$$\frac{n_g}{n_s} \simeq \frac{p_{sg}}{p_{gs}} = \frac{\langle \tau^+ \rangle}{\langle \tau^- \rangle} . \tag{21}$$

In any case, from Eq. (7), we have:

$$\langle l \rangle = (v^+ - v^-)\langle T^+ \rangle + v^- \langle T^- \rangle, \\ \langle T \rangle = \langle T^+ \rangle + \langle T^- \rangle. \tag{22}$$

The ratio of growing to shrinking time is

$$\frac{\langle T^+ \rangle}{\langle T^- \rangle} = \alpha \left(\frac{1 + \frac{\langle l \rangle}{\alpha v \langle T \rangle}}{1 - \frac{\langle l \rangle}{v \langle T \rangle}} \right), \tag{23}$$

where the r.h.s. is expected to stay close to the value α, as l is smaller than $v\langle T^- \rangle$, except for young rods. Because the number of growing time intervals is close to the number of shrinking time intervals, there should not be a large difference between the ratios T^+/T^- and $\langle \tau^+ \rangle/\langle \tau^- \rangle$, suggesting, along with Eq. (21), another relation:

$$\frac{\langle \tau^+ \rangle}{\langle \tau^- \rangle} \simeq \frac{\langle T^+ \rangle}{\langle T^- \rangle} = \frac{n_g}{n_s} \simeq \alpha. \tag{24}$$

To test this relation, we performed a set of simulations with a constant rate of injection $Q_i L_s^2 = 1000$ new rods per simulation step, and varying α. Both n_g, n_s, $\langle \tau^+ \rangle$, $\langle \tau^- \rangle$, T^+ and T^- can be independently obtained from the simulation, as summarized in Fig. 15. The ratio n_g/n_s, T^+/T^-, and $\langle \tau^+ \rangle/\langle \tau^- \rangle$ seems to remain remarkably constant as the simulation goes on. The
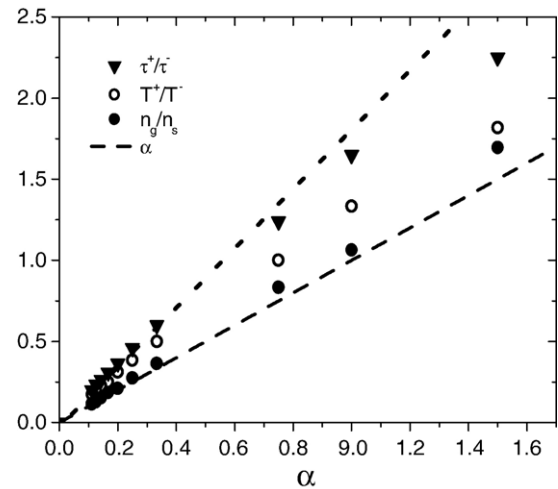

Fig. 15. Horizontal axis: speed ratio $\alpha = v^-/(v^+ - v^-)$. Various curves are represented: the ratio of the times of growth to the times of shrinking $\langle T^+ \rangle/\langle T^- \rangle$, the ratio of intervals of growth and the intervals of shrinking $\langle \tau^+ \rangle/\langle \tau^- \rangle$, the ratio of the number of growing and shrinking rods n_g/n_s and α itself. This Figure illustrates Eq. (24).

agreement is not quantitative, but the four quantities of relation (24) show significant correlations (Fig. 15).

4.4. Anisotropic and non-stationary solutions of the kinetic theory

There are indications that the stationary, homogeneous situation is not the only possible solution of the kinetic theory. We outline in Appendix D, the main features of a *stationary* but *anisotropic* solution, with a non-trivial dependence of p_{gs} in the orientation Ω. This solution can explain why the system tends to choose a preferential global orientation. However, the predicted anisotropy is less than the one that is numerically observed in our system.

The kinetic model described above can also describe time dependent solutions. However, we did not find any simple time-dependent solution compatible with our boundary conditions, i.e. a constant injection rate. It remains that the existence of an unstable, non-stationary and anisotropic solution of the kinetic model cannot be ruled out.

5. Conclusions

We constructed and tested numerically a minimal model of kinetically constrained growth of microtubules which allows for orientation and spatial organization in domain structures. We demonstrated that the collective behavior of the microtubules leads to the formation of bundles of well oriented rods, in the absence of excluded volume interactions and chemical gradients. We suggest this mechanism as a possible alternative in the formation of the oriented and dynamic domains of microtubules observed in experiments [27,31,30,28]. The model is based on the experimental facts, indicating that collisions between microtubules alter their growth rates [27,29] that can provoke the overall ordering.

The kinetic mechanism of collisions distinguish this model from static liquid crystalline ordering driven by excluded volume interactions [34], ordering driven by molecular motors [35,36]

and diffusion based models [13,14,12,37–42], where the spatial organization arises due to synchronous oscillations of microtubules. Oscillations are absent from our model in its current form. Introducing oscillations would require a feedback mechanism between the total mass of microtubules and the speed of growth v^+. Waves of excess and lack of GTP are the driving force for the spatial organization in Reference [38]. In their case all the rods are oriented along a common direction, with the plus ends of the second wave following the minus ends of the first. In our case we obtain domains of different uncorrelated orientations. Within a single domain, the order parameter is very high, and we have a random mixture of parallel and anti-parallel orientations. We speculate that, in the presence of a bias one of the two possible directions will be favored, leading to domains of parallel rods.

In order to single out the influence of the growth mechanism on orientation, we neglected in our model excluded volume interactions and assume homogeneous distribution of positions and angles of microtubules. We use averaged speeds of growth and shrinkage, describing the microtubule dynamics on a coarse-grained level. At this level of approximation we do not distinguish different regimes of microtubule dynamics: phases of constant growth or disassembly, dynamic instability and the treadmilling. We thus have a universal description of microtubules regardless of experimental conditions and implementation, thus suitable for microtubules in general.

The mechanism introduced in our paper is based purely on the mutual influence on the growth and shrinking of the microtubules. Forces also play a role in the interactions between different rods, as demonstrated by several authors. If one considers, at the opposite of the assumptions made in our paper, that there is no induced growth arrest, then the pure effect of forces could also be discussed. For instance, for two isolated microtubules, one hitting the other at some point along its contour, there will be mutual forces which direction and strength depend on the orientations and sizes of each of the rods. The possible outcome will also help the two rods to position parallel to each other, thus helping orientation. However, for concentrations of practical interest for self-organization, each given microtubule is likely to be blocked by its environment, thus reducing the efficiency of such force orientation mechanism.

We tested the responsive properties of the system to some external stress. We found that the alignment was much faster in the presence of any small anisotropic bias. This result is interesting in the context of the influence of the gravitational field on the microtubule orientation [16,18,30,39,40,43]. In this paper we did not discuss extensively the relationship between gravity and possible bias effects, we rather postpone the discussion for later work. The difficulty resides in the weak coupling between gravity and microtubule motion or orientation. Previous authors [40] dealt with this difficulty by invoking the gravitation drift leading to the motion of microtubule bundles. Such mechanism can be invoked as well in our case, and would obviously favor the growth of microtubules oriented upwards. A different orientation bias could also originate at the boundaries, if the microtubules orientation was influenced by the presence of the walls. Similar effects have been noted by others [20,44,26].

Along with simulations, we developed a kinetic theory which accounts for the basic scaling properties of the system: con-

version rates and average length of the microtubules. The quantitative agreement remains poor, due to the strong correlations present in this two-dimensional system, in which the emergence of large anisotropic domains is incompatible with the homogeneity assumption ($\overrightarrow{r}$ independence).

Our system consumes energy since the unidirectional growth of microtubules breaks detailed balance, a typical out of equilibrium situation. Exhausting the source of energy will lead to disassembly of microtubules regardless their orientation. When the rate of growth approaches the rate of shrinkage, it takes longer time to orient microtubules.

Because we were able to show that this mechanism also induces some alignment in three dimension, we believe that our kinetic theory would give a better agreement in higher dimensional systems, which is the subject of future work.

Acknowledgments

Appendix A. A kinetic theory for homogeneous distributions

We assume first that the system is homogeneous, and that the distribution functions do not depend on $\overrightarrow{r}$. Denoting by S the area of the system, the distribution functions then reduce to their homogeneous form:

$$c_{g,s,t}(l, \Omega, \overrightarrow{r}, t) = \frac{1}{S} c_{g,s,t}(l, \Omega, t). \tag{A.1}$$

The functions $c_{g,s,t}$ are "extensive" functions of the area S. We propose a master equation for these functions, which accounts for the shrinking and growing behavior of the rods, and also accounts for the possibility of interconversion between the s- and g-states. In order to cope with a possible global anisotropy of the rods, we let the interconversion rates depend on the orientation Ω, but not on the length: $p_{gs}(\Omega)dt$ is the fraction of g-rods which switches to a s-rod state during the time interval dt, while $p_{sg}(\Omega)dt$ describes the reverse change. The corresponding master equation reads:

$$\begin{cases} c_g(l, \Omega, t+dt) = c_g(l - vdt, \Omega, t) + p_{sg}(\Omega)c_s(l, \Omega, t)dt - p_{gs}(\Omega)c_g(l, \Omega, t)dt; \\ c_s(l, \Omega, t+dt) = c_s(l + v^- dt, \Omega, t) + p_{gs}(\Omega)c_g(l, \Omega, t)dt - p_{sg}(\Omega)c_s(l, \Omega, t)dt. \end{cases} \tag{A.2}$$

The continuous limit $dt \rightarrow 0$ leads to a system of two partial differential equations:

$$\begin{cases} \dfrac{\partial c_g}{\partial t} + v \dfrac{\partial c_g}{\partial l} = p_{sg}c_s - p_{gs}c_g; \\ \dfrac{\partial c_s}{\partial t} - \alpha v \dfrac{\partial c_s}{\partial l} = p_{gs}c_g - p_{sg}c_s. \end{cases} \tag{A.3}$$

where appears the ratio $\alpha = v^- / v = v^- / (v^+ - v^-)$.

The partial derivatives in the left hand sides of Eq. (A.3), correspond to a drift motion of the rods along the l axis. We can associate to this drift the "currents" of growing $j_g(l, \Omega, t) = vc_g$ and

shrinking $j_s(l, \Omega, t) = -\alpha v c_s$ rods. The sum $j_g + j_s$ measures the difference between the number of rods which have grown bigger than l, and the number of rods which have shrunk below l. The distribution $c_t = c_g + c_s$ obeys a usual conservation equation $\partial c_t / \partial t + \partial (j_g + j_s) / \partial l = 0$, provided $l > 0$.

In particular, as there is no other option for a rod with length 0 than growing or disappearing, and our master equations must be completed with a boundary condition involving j_g and the injection rate Q_i.

$$Q_i(\Omega) = v c_g(l = 0, \Omega). \tag{A.4}$$

Meanwhile, the rate of disappearance of the rods is Q_d, obeying

$$Q_d(\Omega) = \alpha v c_s(l = 0, \Omega). \tag{A.5}$$

At the other extreme, we expect that

$$\lim_{l \to \infty} c_{g,s,t}(l, \Omega) = 0. \tag{A.6}$$

Eqs. (A.2), (A.4), and (A.6) are the basis of our kinetic theory.

Appendix B. The stationary case

The above system of equations is simpler if we look for a time independent solution, setting the time partial derivative to zero. Introducing $c_t = c_g + c_s$, and $c_d = c_g - c_s$, we get:

$$\begin{cases} \frac{v}{2}(1 - \alpha)\frac{\partial c_t}{\partial l} + \frac{v}{2}(1 + \alpha)\frac{\partial c_d}{\partial l} = 0; \\ \frac{v}{2}(1 - \alpha)\frac{\partial c_d}{\partial l} + \frac{v}{2}(1 + \alpha)\frac{\partial c_t}{\partial l} = (p_{sg} - p_{gs})c_t - (p_{sg} + p_{gs})c_d; \\ c(0, \Omega) = q; \lim_{l \to \infty} c(l, \Omega) = 0, \end{cases} \tag{B.1}$$

with solution

$$\begin{cases} c_t(l, \Omega) = q e^{-l/\bar{l}(\Omega)}; \\ c_d(l, \Omega) = \frac{\alpha - 1}{1 + \alpha} q e^{-l/\bar{l}(\Omega)}, \end{cases} \tag{B.2}$$

where, for convenience, we have introduced $q = c_t(0, \Omega)$, while the average length in the direction Ω is given by:

$$\bar{l}(\Omega) = \frac{\alpha v}{\alpha p_{gs}(\Omega) - p_{sg}(\Omega)}. \tag{B.3}$$

Moreover, the distributions c_g and c_s verify

$$\frac{c_g(l, \Omega)}{c_s(l, \Omega)} = \alpha, \tag{B.4}$$

and consequently,

$$\begin{aligned} c_g &= \frac{\alpha q}{\alpha + 1} e^{-l/\bar{l}(\Omega)}; \\ c_s &= \frac{q}{\alpha + 1} e^{-l/\bar{l}(\Omega)}. \end{aligned} \tag{B.5}$$

Finally, the injection rate $Q_i(\Omega)$ is related to $q(\Omega)$ by

$$Q_i(\Omega) = \frac{\alpha}{\alpha + 1} v q(\Omega), \tag{B.6}$$

which is the basis of a stationary, homogeneous solution of the system, expressed in terms of Q_i, α, p_{gs} and p_{sg}. An example of explicit angular dependence of $Q_t(\Omega)$ is the situation described in Section 3.2 and in Fig. 4. In most cases, however, we are interested in an isotropic, constant, function Q_i, which we consider now.

To move further, we must estimate the interconversion rates p_{gs} and p_{sg}. To estimate p_{sg}, we assume that collisions are pairwise, and, as in the usual kinetic theory of gases, that there is no correlation between any two colliding rods. Then, p_{sg} does not depend on angles, and is inversely proportional to the average waiting time $\langle \tau^- \rangle$ spent in the blocked state. Since all rods shrink at the same speed, the waiting time depends only on the distance between the contact point and the minus end of the restricting rod. Assuming a uniform distribution of contact points along the rod, we find that the average waiting time associated to a restricting rod with length l is $l/(2v^-)$, and consequently,

$$\langle \tau^- \rangle = \frac{\bar{l}}{2v^-}; p_{sg} = \frac{1}{\langle \tau^- \rangle} = \frac{2v^-}{\bar{l}}. \tag{B.7}$$

In this equation, we need to know the average length $\bar{l}$ of the rods, irrespective of their orientation. Given the solution obtained above, this simply reads:

$$\bar{l} = \frac{\int dl d\Omega l \, c_t(l, \Omega)}{\int dl d\Omega c_t(l, \Omega)} = \frac{\int d\Omega \left(\bar{l}(\Omega)\right)^2}{\int d\Omega \bar{l}(\Omega)}. \tag{B.8}$$

The estimate of p_{gs} also comes from the analogy with the kinetic theory of gases. We imagine the system from the point of view of an observer sitting at the top of a growing tip, and estimate the area swept by the mesh of all the other rods, moving relatively to the observer at speed $-v^+$. The typical collision time is reached when this area becomes comparable to the total area S of the system, making the probability of collision of order one. The calculation shows that the collision time depends on the projected length l' of the obstructing rod, and on the relative orientation difference $\Omega - \Omega'$ between the two rods. We can write:

$$\bar{l}_p(\Omega) = \frac{\int d\Omega' dl' l' |\sin(\Omega - \Omega')| c_t(l', \Omega')}{\int d\Omega' dl' c_t(l', \Omega')}, \tag{B.9}$$

and the probability $p_{gs}(\Omega)$ reduces to:

$$p_{gs}(\Omega) = v^+ \bar{l}_p(\Omega) \left(\frac{n_t}{S}\right), \tag{B.10}$$

where S is the total area of the system, n_t is the total number of rods, and (n_t/S) is the ratio of two "extensive" functions.

Appendix C. The isotropic solution and its predictions

The isotropic hypothesis consists in taking p_{gs} and p_{sg} angle independent. This simplifies the above kinetic theory to a point where a self-consistent analytical solution becomes available. The Ω dependence of $\bar{l}$ and $\bar{l}_p$ drops out, and we get:

$$\bar{l}_p = \frac{2\bar{l}}{\pi}, \tag{C.1}$$

and Eq. (B.3) leads to the self-consistence relations:

$$\bar{l} = \frac{\alpha v}{\alpha v + \frac{n_t}{S}\frac{2\bar{l}}{\pi} - \frac{2v^-}{\bar{l}}}; \tag{C.2}$$

$$(\bar{l})^2 = \frac{3\pi}{2(\alpha + 1)}\frac{S}{n_t}. \tag{C.3}$$

Then, we replace n_t by $\frac{\alpha + 1}{\alpha}\frac{Q_i\,\bar{l}}{v}$, to make a prediction for the average length $\bar{l}$ and the number of rods n_t.

$$\bar{l} = \sqrt{\frac{3\pi}{2(\alpha + 1)}\frac{S}{n_t}} \simeq \left(\frac{S}{n_t}\right)^{\frac{1}{2}}; \tag{C.4}$$

$$\bar{l} = \sqrt[3]{\frac{3\alpha}{4(\alpha + 1)^2}\frac{Sv}{Q_i}} \simeq \left(\frac{Sv}{Q_i}\right)^{\frac{1}{3}}; \tag{C.5}$$

$$n_t = 2\pi\frac{\alpha + 1}{\alpha v}\bar{l}Q_i. \tag{C.6}$$

Appendix D. The anisotropic solution

We believe that the system of Eqs. (B.3), (B.7), (B.8), (B.9), and (B.10) also admits an anisotropic solution, characterized by an explicit Ω dependence of $p_{gs}(\Omega)$ and $\bar{l}(\Omega)$ while p_{sg} remains isotropic. To approach this solution, we expand $\bar{l}(\Omega)$ in cosine series:

$$\bar{l}(\Omega) = l_0 + l_2\cos(2\Omega) + l_4\cos(4\Omega)... \tag{D.1}$$

and approximate $\sin|\Omega - \Omega'|$ in a similar manner:

$$\sin|\Omega| = s_0 + s_2\cos(2\Omega) + s_4\cos(4\Omega)... \tag{D.2}$$

Possible choices include the Fourier expansion:

$$\sin|\Omega| = \frac{2}{\pi} - \frac{4}{\pi}\sum_{p=1}^{\infty}\frac{\cos(2p\Omega)}{4p^2 - 1}, \tag{D.3}$$

or replacing $\sin|\Omega|$ by $\sin^2(\Omega)$.

For instance, by keeping the two first terms in the expansion, and writing the self-consistence Eq. (B.3) under the form $\bar{l}(\Omega) \times (\alpha p_{gs}(\Omega) - p_{sg}) = \alpha v$, we finally obtain a system of equations for l_0 and $x = l_2/l_0$:

$$\frac{\alpha v + n_t l_0^2}{S}\left(s_0\left[1 + \frac{x^2}{2}\right] + s_2\frac{x^2}{2}\right) = 3v^-;$$

$$\frac{\alpha v + n_t l_0^2}{S}\left(s_0 x\left[1 + \frac{x^2}{2}\right] + s_2 x\right) = \frac{2v^- x}{1 + \frac{x^2}{2}}. \tag{D.4}$$

We observe that the isotropic solution $x = 0$, $l_2 = 3Sv^-/(s_0\alpha v^+ n_t)$ (equivalent to Eq. (C.3)) coexists along with an anisotropic solution $x \neq 0$, where x solves

$$\frac{\alpha v + n_t l_0^2}{S}\left(s_0\left[1 + \frac{x^2}{2}\right] + s_2\right) = \frac{2v^-}{1 + \frac{x^2}{2}}, \tag{D.5}$$

and l_0 is a function of x and the other parameters of the problem.

Thus, despite its strong mean field features, the kinetic model is compatible with the emergence of an anisotropic solution, with an explicit angular dependence of the average length of the rods. However, this anisotropy is bounded, with an average length finite in all directions, while the domains observed in the simulations can grow without limit.

Appendix E. Supplementary data

Supplementary data associated with this article can be found, in the online version, at doi:10.1016/j.bpc.2007.04.009.

References

[1] J. Howard, Mechanics of Motor Proteins and the Cytoskeleton, Sinauer Associates Inc., Sunderland, 2001.
[2] S. Gadde, R. Heald, Mechanisms and molecules of the review mitotic spindle, Curr. Biol. 14 (2004) R797–R805.
[3] A.A. Hyman, E. Karsenti, Morphogenetic properties of microtubules and mitotic spindle assembly, Cell 84 (1996) 401–410.
[4] A. Desai, T.J. Mitchison, Microtubule polymerization dynamics, Annu. Rev. Cell Dev. Biol. 13 (1997) 83–117.
[5] O.N.V. Caudron, D. Job, Microtubule dynamics, CMLS 58 (2001) 2069–2084.
[6] J. Canaday, V. Stoppin-Mellet, J. Mutterer, A.M. Lambert, A.C. Schmit, Higher plant cells: gamma-tubulin and microtubule nucleation in the absence of centrosomes, Microsc. Res. Tech. 49 (2000) 487–495.
[7] T. Murata, S. Sonobe, T.I. Baskin, S. Hyodo, S. Hasezawa, T. Nagata, T. Horio, M. Hasebe, Microtubule-dependent microtubule nucleation based on recruitment of γ-tubulin in higher plants, Nat. Cell Biol. 7 (2005) 961–968.
[8] J.W. Vos, M. Dogterom, A.M.C. Emons, Microtubules become more dynamic but not shorter during preprophase band formation: a possible "search-and-capture" mechanism for microtubule translocation, Cell Motil. Cytoskelet. 57 (2004) 246–258.
[9] I.E. Maly, Diffusion approximation of the stochastic process of microtubule assembly, Bull. Math. Biol. 64 (2002) 213–238.
[10] I.M. Janosi, D. Chretien, H. Flyvbjerg, Structural microtubule cap: stability, catastrophe, rescue, and third state, Biophys. J. 83 (2002) 1317–1330.
[11] A. Krebs, K.N. Goldie, A. Hoenger, Structural rearrangements in tubulin following microtubule formation, EMBO Rep. 6 (2005) 227–232.
[12] R. Melki, M.-F. Carlier, D. Pantaloni, Oscillations in microtubule polymerization: the rate of gtp regeneration on tubulin controls the period, EMBO J. 7 (9) (1988) 2653–2659.
[13] E.M. Mandelkow, E. Mandelkow, Microtubule oscillations, Cell Motil. Cytoskelet. 22 (1992) 235–244.
[14] A. Marx, E. Mandelkow, A model of microtubule oscillations, Eur. Biophys. J. Biophys. Lett. 22 (6) (1994) 405–421.
[15] J. Tabony, D. Job, Gravitational symmetry breaking in microtubular dissipative structures, Proc. Natl. Acad. Sci. U. S. A. 89 (1992) 6948–6952.
[16] J. Tabony, Self-organization in a simple biological system through chemically dissipative processes, Nanobiology 4 (1996) 117–137.
[17] N. Glade, J. Tabony, Brief exposure to high magnetic fields determines microtubule self-organisation by reaction–diffusion processes, Biophys. Chemist. 115 (2005) 29–35.
[18] J. Tabony, N. Glade, J. Demongeot, C. Papaseit, Biological self-organization by way of microtubule reaction–diffusion processes, Langmuir 18 (2002) 7196–7207.
[19] N. Glade, E. Beaugnon, J. Tabony, Ground-based methods reproduce space-flight experiments and show that weak vibrations trigger microtubule self-organisation, Biophys. Chemist. 121 (1) (2006) 1–6.
[20] S. Cortes, N. Glade, I. Chartier, J. Tabony, Microtubule self-organisation by reaction–diffusion processes in miniature cell-sized containers and phospholipid vesicles, Biophys. Chemist. 120 (3) (2006) 168–177.
[21] V.A. Baulin, A.R. Khokhlov, Nematic ordering of rigid rods in a gravitational field, Phys. Rev., E Stat. Phys. Plasmas Fluids Relat. Interdiscip. Topics 60 (1999) 2973–2977.

[22] V.A. Baulin, Self-assembled aggregates in the gravitational field: growth and nematic order, J. Chem. Phys. 119 (2003) 2874–2885.

[23] M. Dogterom, B. Yurke, Measurement of the force–velocity relation for growing microtubules, Science 278 (1997) (1997) 856–860.

[24] M. Dogterom, M.E. Janson, C. Faivre-Moskalenko, A. van der Horst, J.W.J. Kerssemakers, C. Tanase, B.M. Mulder, Force generation by polymerizing microtubules, Appl. Phys., A 75 (2002) 331–336.

[25] P. Dhonukshe, J.T.W.J. Gadella, Alteration of microtubule dynamic instability during preprophase band formation revealed by yellow fluorescent protein–clip170 microtubule plus-end labeling, Plant Cell 15 (2003) 597–611.

[26] P. Bastiaens, M. Caudron, P. Niethammer, E. Karsenti, Gradients in the self-organization of the mitotic spindle, Trends Cell Biol. 16 (2006) 125–134.

[27] R. Dixit, R. Cyr, Encounters between dynamic cortical microtubules promote ordering of the cortical array through angle-dependent modifications of microtubule behavior, Plant Cell 16 (2004) 3274–3284.

[28] N. van Bruaene, G. Joss, P. van Oostveldt, Reorganization and in vivo dynamics of microtubules during *Arabidopsis* root hair development, Plant Physiol. 136 (2004) 3905–3919.

[29] C.L. Wymer, D.D. Fisher, R.C. Moore, R.J. Cyr, Elucidating the mechanism of cortical microtubule reorientation in plant cells, Cell Motil. Cytoskelet. 35 (1996) 162–173.

[30] R. Himmelspach, C. Wymer, C.W. Lloyd, P. Nick, Gravity-induced reorientation of cortical microtubules observed in vivo, Plant J. 18 (1999) 449–453.

[31] C.W. Lloyd, R. Himmelspach, P. Nick, C. Wymer, Cortical microtubules form a dynamic mechanism that helps regulate the direction of plant growth, Grav. Space Biol. Bull. 13 (2000) 59–66.

[32] I.A. Vorobjev, V.I. Rodionov, I.V. Maly, G.G. Borisy, Contribution of plus and minus end pathways to microtubule turnover, J. Cell Sci. 112 (1999) 2277–2289.

[33] A.J. Bray, Theory of phase ordering kinetics, Adv. Phys. 43 (1994) 357–459.

[34] L. Onsager, Ann. N.Y. Acad. Sci. 51 (1949) 627.

[35] E. Karsenti, F. Nedelec, The mitotic spindle and actin tails, Biol. Cell 96 (2004) 237–240.

[36] B. Bassetti, M.C. Lagomarsino, P. Jona, A model for the self-organization of microtubules driven by molecular motors, Eur. Phys. J., B Cond. Matter Phys. 15 (2000) 483–492.

[37] C. Robert, M. Bouchiba, R. Robert, R. Margolis, D. Job, Self-organization of the microtubule network: a diffusion based model, Biol. Cell 68 (1990) 177–181.

[38] N. Glade, J. Domongeot, J. Tabony, Numerical simulations of microtubule self-organization by reaction and diffusion, Acta Biotheor. 50 (2002) 239–268.

[39] S. Portet, J.A. Tuszynski, J.M. Dixon, M.V. Sataric, Models of spatial and orientational self-organization of microtubules under the influence of gravitational fields, Phys. Rev., E Stat. Phys. Plasmas Fluids Relat. Interdisc. Topics 68 (2003) 021903.

[40] J.A. Tuszynski, M.V. Sataric, S. Portet, J.M. Dixon, Physical interpretation of microtubule self-organization in gravitational fields, Phys. Lett., A 340 (2005) 175–180.

[41] P.A. Deymier, Y. Yang, J. Hoying, Effect of tubulin diffusion on polymerization of microtubules, Phys. Rev., E Stat. Phys. Plasmas Fluids Relat. Interdisc. Topics 72 (2005) 021906.

[42] D. Sept, Model for spatial microtubule oscillations, Phys. Rev., E Stat. Phys. Plasmas Fluids Relat. Interdisc. Topics 60 (1) (1999) 838–841.

[43] R. Himmelspach, P. Nick, Gravitropic microtubule reorientation can be uncoupled from growth, Planta 212 (2001) 184–189.

[44] I.V. Maly, G.G. Borisy, Self-organization of treadmilling microtubules into a polar array, Trends Cell Biol. 12 (10) (2002) 462–465.